Lab on a Chip

PAPER

View Article Online
View Journal | View Issue

Cite this: *Lab Chip*, 2017, **17**, 460

Pinch-off dynamics and dripping-onto-substrate (DoS) rheometry of complex fluids†

Jelena Dinic, Leidy Nallely Jimenez and Vivek Sharma*

Liquid transfer and drop formation/deposition processes involve complex free-surface flows including the formation of columnar necks that undergo spontaneous capillary-driven instability, thinning and pinch-off. For simple (Newtonian and inelastic) fluids, a complex interplay of capillary, inertial and viscous stresses determines the nonlinear dynamics underlying finite-time singularity as well as self-similar capillary thinning and pinch-off dynamics. In rheologically complex fluids, extra elastic stresses as well as non-Newtonian shear and extensional viscosities dramatically alter the nonlinear dynamics. Stream-wise velocity gradients that arise within the thinning columnar neck create an extensional flow field, and many complex fluids exhibit a much larger resistance to elongational flows than Newtonian fluids with similar shear viscosity. Characterization of pinch-off dynamics and the response to both shear and extensional flows that influence drop formation/deposition in microfluidic and printing applications requires bespoke instrumentation not available, or easily replicated, in most laboratories. Here we show that dripping-onto-substrate (DoS) rheometry protocols that involve visualization and analysis of capillary-driven thinning and pinch-off dynamics of a columnar neck formed between a nozzle and a sessile drop can be used for measuring shear viscosity, power law index, extensional viscosity, relaxation time and the most relevant processing timescale for printing. We showcase the versatility of DoS rheometry by characterizing and contrasting the pinch-off dynamics of a wide spectrum of simple and complex fluids: water, printing inks, semi-dilute polymer solutions, yield stress fluids, food materials and cosmetics. We show that DoS rheometry enables characterization of low viscosity printing inks and polymer solutions that are beyond the measurable range of commercially-available capillary break-up extensional rheometer (CaBER). We show that for high viscosity fluids, DoS rheometry can be implemented relatively inexpensively using an off-the-shelf digital camera, and for many complex fluids, similar power law scaling exponent describes both neck thinning dynamics and the shear thinning response.

Received 15th September 2016,
Accepted 13th December 2016

DOI: 10.1039/c6lc01155a

www.rsc.org/loc

I. Introduction

The rapid, repeated, precise formation/deposition of drops[1–4] and printing or patterning of small features (say $l = 10^{-3}$–1 mm)[3–9] are of great importance to a variety of old and new industrial applications. Microfluidics and lab-on-chip devices provide an exquisite method for forming droplets and particles,[10–13] encapsulating cells, biomarkers and pharmaceuticals,[14,15] and for formulating multicomponent emulsions.[16–18] Significant recent interest lies in adopting printing (inkjet, gravure, roll-to-roll, *etc.*) and coating (dip-, slot-, doctor blade, *etc.*) technologies for liquid transfer and precise deposition of unconventional materials, *e.g.*: printed solar cells,[7,19–23] print electronics,[8,24–26] ink-jet printed scaffolds, cells, biosensors, and tissues,[9,27–31] creating printed DNA or protein arrays,[27] microfluidic devices,[32] polymeric and inorganic membranes,[33] rapid prototyping using 3-D printing,[34] and additive manufacturing.[4,27,35,36] Classical inkjet printing and microfluidic drop formation devices rely on drop formation from lower viscosity ($\eta \sim$ 5–20 mPa s) formulations with a Newtonian fluid-like shear rheology.[2,10] Many comprehensive reviews describe the complex interplay of inertial, viscous and capillary stresses that dictates the nonlinear dynamics underlying finite-time singularity, capillary-thinning dynamics and satellite drop formation for simple, Newtonian fluids.[1,2,37–39] In contrast, due to the presence of additional viscoelastic stresses, microstructural transitions and non-Newtonian shear and extensional viscosity, describing free surface flows associated with drop formation or dispensing of rheologically-complex fluids presents several challenges.[1,40–44] For example, complex fluids with nearly indistinguishable response to shear flow, often exhibit vast differences in their printability, due to the difference in pinch-

Department of Chemical Engineering, University of Illinois at Chicago, IL 60607, USA. E-mail: viveks@uic.edu

† Electronic supplementary information (ESI) available. See DOI: 10.1039/c6lc01155a

off dynamics correlated with underlying microstructural transitions and extensional rheology behavior.[43–46] In this contribution, we characterize such differences using dripping-onto-substrate (DoS) rheometry,[46] which relies on the visualization and analysis of capillary-driven thinning of the neck in an asymmetric liquid bridge created by releasing a drop onto a substrate. We show the DoS rheometry protocols allow a quantitative characterization of rheological measures like shear viscosity, power law index, extensional viscosity, extensional relaxation time as well as the processing timescales relevant for printing application for an entire spectrum of complex fluids.

Free-surface flows, with strong capillary stresses and surface-tension driven instabilities,[1–3,37–39] accompany printing of small feature sizes and influence precision, speed and quality of patterns and structures formed.[2–4,19,20] Strong extensional kinematics associated with stream-wise gradients in velocity field often develop in free surface flows near curved surfaces in coating flows[40] and in fluid necks undergoing capillary-driven thinning[44–50] in ink-jet printing, gravure printing, spraying and splashing. Strong extensional flows can result in large conformational changes, even full extension of polymer chains, altering their relaxation dynamics as well as the resistance to the extensional flow field quantified as extensional viscosity.[44–50] Likewise, strong extensional flows can cause stretching and break-up of drops, bubbles and vesicles,[51] unfolding, uncoiling of proteins and macromolecules,[52–54] and disruption of microstructure, potentially influencing the structure and properties of printed or dispensed emulsions and foams, printed electronics and photovoltaics,[8,19,20] cell- or protein-based biofluids.[27–30] Multicomponent complex fluids provide a much larger resistance to extensional flow than expected on the basis of their shear viscosity, thus influencing processing timescales as well as primary and satellite drop formation. For a Newtonian fluid, the extensional viscosity is a factor of three times larger than the shear viscosity (as was first shown by Trouton[55]); however it can be several orders of magnitude higher for complex fluids containing polymers,[42–47] wormlike micelles,[56–59] and non-spherical particles or fibers.[60–62] Therefore, the understanding of the extensional response of complex fluids, especially in the context of pinch-off dynamics, is a necessary step to arrive at a rational basis for choosing or designing inks or selecting processing parameters for microfluidic drop/particle formation and printing applications.

Quantitative analysis of the capillary-thinning and pinch-off dynamics of complex fluids provides a measure of the extensional viscosity and the characteristic processing timescale relevant for capillary-driven flows.[44–50,56–67] Self-thinning of a stretched liquid bridge formed by applying a discrete step-strain to a drop between two parallel plates,[63–67] is utilized in a commercially-available device called Capillary Break-up Extensional Rheometer (CaBER).[44,47,68,69] The extensional rate determined by self-similar thinning of neck grows unbounded and diverges before pinch-off for inviscid, viscous and power-law fluids,[44] but attains a constant value determined by an apparent, material-dependent relaxation time during elastocapillary thinning. Capillary thinning analysis also forms the basis of a jetting-based rheometry technique called Rayleigh Ohnesorge Jetting Extensional Rheometer (ROJER),[45] that relies on an understanding of the influence of elasticity of nonlinear fluid dynamics and convective capillary-driven instability.[45,70–74] So far, only weakly viscoelastic polymer solutions have been characterized with ROJER,[45,72] and jetting-based rheometry studies on complex fluids with higher viscosity and higher elasticity remain an open challenge. Progressive thinning of the neck radius appears to be self-similar for inviscid, Newtonian fluids in dripping, where the pinch-off results from the interplay of gravitational drainage and capillarity,[2,49,50,75–77] but sensitivity to drop volume is observed in elastocapillary response of dilute polymer solutions. Furthermore the visualization of the thinnest radius is quite challenging in dripping as long-lived threads form for higher viscosity and highly viscoelastic fluids.[49,50,75–77] The dripping-onto-substrate (DoS) rheometry protocols preserve the simplicity of a dripping set-up, and hence can be replicated and emulated relatively easily, and quite inexpensively for high viscosity fluids, as shown in the current contribution. Furthermore, the presence of underlying substrate in DoS rheometry facilitates visualization of a fixed Eulerian location of thinning neck, and as the stretched-liquid bridge configuration is quite similar to CaBER, similar force balances and scaling laws apply.

In this contribution, we outline the experimental protocols underlying the dripping-onto-substrate (DoS) rheometry, describing imitable methods used for creating, visualizing and analyzing capillary-driven thinning and pinch-off dynamics of a stretched neck formed between a pendant drop attached to dispensing nozzle and a sessile drop deposited on a substrate beneath it. In a previous contribution[46] focused on measuring extensional relaxation times of dilute polymer solutions, we refered to this technique as optically-detected elastocapillary self-thinning dripping-onto-substrate (ODES-DOS) extensional rheometry, for we primarily focused on the analysis of the elastocapillary self-thinning as displayed by change in optically-detected neck radius. While the radius is still optically-detected, in this contribution, we apply the dripping-onto-substrate rheometry protocols more extensively and generally for investigating a wide range of fluids that display inertio-capillary thinning (water), viscocapillary thinning (glycerol/water mixtures, honey, chocolate syrup), power law thinning (photovoltaic ink, mayonnaise, ketchup, conditioner, Carbopol solutions) and elastocapillary thinning (polymer solutions). We showcase the versatility of DoS rheometry, highlighting the difference in pinch-off dynamics and printability displayed by representative complex fluids, including polymer solutions, emulsions, wormlike micellar solutions and particle-laden fluids often used in paints, coatings, cosmetics and food industry. We contend that DoS rheometry provides one of the cheapest methods for measuring viscosity for Newtonian fluids, relaxation time for polymer solutions, and for exploring differences in drop formation and printing

behavior of low viscosity inks as well as power law fluids (*e.g.* food, cosmetics and coatings) where characterizing extensional rheology is most challenging, and yet necessary, for designing products.

II. Experimental: dripping-onto-substrate (DoS) rheometry

The dripping-onto-substrate (DoS) rheometry requires an imaging set-up and a liquid dispensing system, shown schematically in Fig. 1. A stretched liquid bridge is formed between a sessile drop and a nozzle by dripping-onto-substrate, *i.e.* by releasing a finite volume of fluid from a nozzle onto a glass substrate. The nozzle is placed above the substrate at distance H from the substrate, and the optimal aspect ratio (H/D_0) is around 3. The fluid is dispensed using a syringe pump, and the pumping is stopped at the instant when the drop contacts the interface. As dripping occurs at relatively low flow rates, the approach of the drop can be tracked in real time. Slow release of drops onto a partial wetting substrate (spreading parameter $S < 0$ and contact angle $\theta < 90°$) helps to decouple the neck thinning dynamics from the drop spreading dynamics. Alternatively, the contact line of the drop formed on the substrate can be pinned by using a cylindrical plate in analogy with the CaBER configuration. We have verified that for drop diameter smaller than the capillary length, the characteristic response of viscous and viscoelastic fluids is not affected by a change in nozzle diameter, flow rate within the nozzle, and the aspect ratio (as long as unstable liquid bridge is formed[44]). The imaging system used for visualization and analysis of low viscosity fluid consists of a high-speed camera (Fastcam SA3), magnification lenses (Nikkor 3.1× zoom (18–55 mm) and a super macro lens) and a halogen light source with a diffuser for producing backlit images. Variable frame rates 250–20 000 fps (frames per second) are used for imaging with the high-speed camera.

We show here that for high viscosity fluids the DoS rheometry can be recreated using a commercial, off-the-shelf, digital-SLR camera (Nikon D5200, frame rate ≤60 fps). The DoS videos were analyzed using ImageJ[78] and MATLAB with specially written codes for analyzing thinning and pinch-off dynamics. The size of symbols in all the plots shown in this study is of the same order (typical 10 μm) as the error estimated based on the resolution of the imaging system and the analysis protocols. The surface tension, σ of fluids used is measured, if needed, using pendant drop analysis tensiometry. Relatively low shear rates ($<1\ s^{-1}$) are encountered within the stainless steel nozzle (inner and outer diameters, D_i = 0.838 mm and D_0 = 2 R_0 = 1.27 mm) for flow rate Q = 0.02 ml min^{-1} used in this study. In contrast, much higher shear rates values ($>10^3\ s^{-1}$) and a pre-stretch are quite typical within the nozzle during jetting-based rheometry studies. Likewise, the initial step strain in CaBER, provides a pre-stretch that can influence pinch-off dynamics for polymer solution as well as for highly structured fluids.[56,79] Recently, Campo-Deano and Clasen[80] modified CaBER protocol to create a slow retraction method (SRM) that involves a slow initial extension of liquid bridge to minimize inertial oscillations, and the modification enabled them to access shorter relaxation time than possible with conventional CaBER that uses a step-strain. The slow release of drop in DoS rheometry likewise minimizes inertial oscillations and therefore the protocols are suitable for studies on low viscosity inks, as discussed in the next section.

III. Results and discussion

Pinch-off dynamics of printing inks and model Newtonian fluids

Capillary thinning and pinch-off dynamics of representative (commercially-available) printing inks and low viscosity fluids like water can be visualized and analyzed using dripping-onto-substrate (DoS) rheometry as shown in Fig. 2a. The

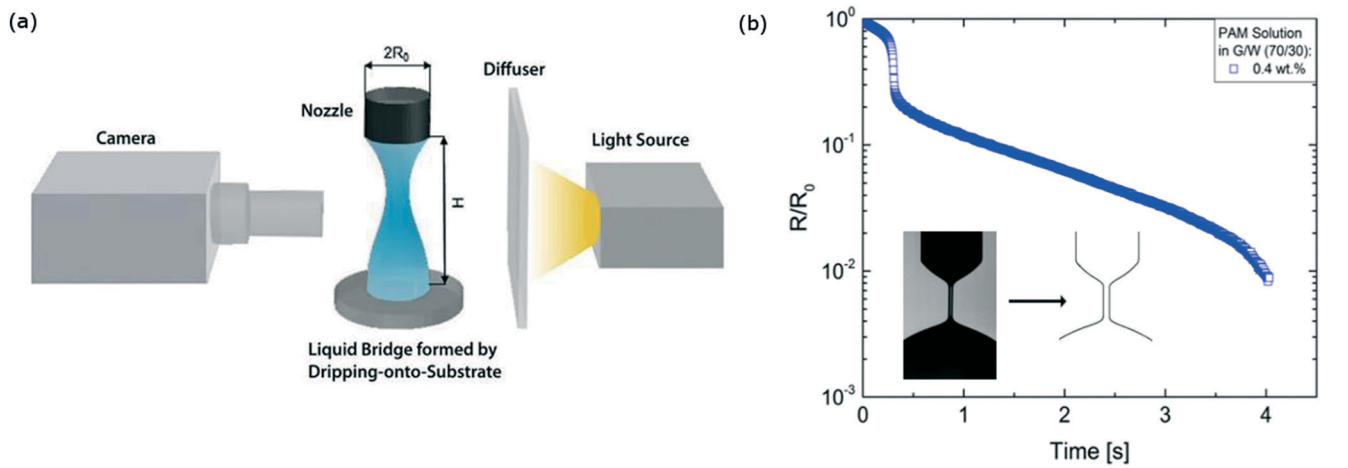

Fig. 1 Dripping-onto-Substrate (DoS) rheometry. a) The experimental setup consists of a an imaging system that includes a light source, a diffuser and a high-speed camera and a dispensing system that includes a syringe pump used for pumping fluids through a nozzle placed height, H above the glass substrate. b) Neck shape evolution and radius evolution as a function of time are obtained by analyzing movies frame by frame using MATLAB. Example shown is for a polyacrylamide (PAM) solution in a glycerol/water mixture.

radius evolution data is plotted for three commercial ink samples including two aqueous PEDOT:PSS suspensions (prepared from a stock aqueous solution containing 3–4% PEDOT:PSS and reported viscosity of 10–30 cP; Sigma-Aldrich) and a black graphic ink used in inkjet printer (particle-laden ink, sourced from freshinkjets.com). The inkjet printing inks are typically optimized to have a low viscosity ($\eta < 20$ mPa s), high surface tension (>30 mN m^{-1}), and a nearly Newtonian response to shear flow.[2,39] Since the PEDOT:PSS inks are formed by diluting a low viscosity aqueous stock solution and the printer ink has low viscosity by design, the radius evolution datasets show that DoS rheometry can be used for characterization of low viscosity printable fluids. In contrast, characterization of capillary thinning and pinch-off dynamics for low viscosity ($\eta < 20$ mPa s), weakly viscoelastic ($\eta < 1$ ms) fluids are inaccessible in CaBER as the pinch-off is completed even before the typical commercial instruments can stretch the liquid bridge,[44,45,68,72,80] and inertial effects from the initial step-strain create oscillations that can influence neck thinning dynamics.

The shape of the neck and the neck thinning dynamics of inks (see Fig. 2b) discerned from movies show qualitative differences from the model Newtonian fluids including pure water (Fig. 2a) and higher viscosity glycerol/water mixtures (Fig. 2c). The neck profile for water, becomes self-similar, and displays a cone angle of 18.1° in agreement with theory,[81,82] in frames leading to the pinch-off. Though close to the pinch-off point, the angles seem to be close to 18.1° for these low viscosity ink samples, the overall shape of the neck looks quite different (see Fig. 2b). Quantitative analysis of the radius evolution data or neck thinning dynamics for water, a low viscosity

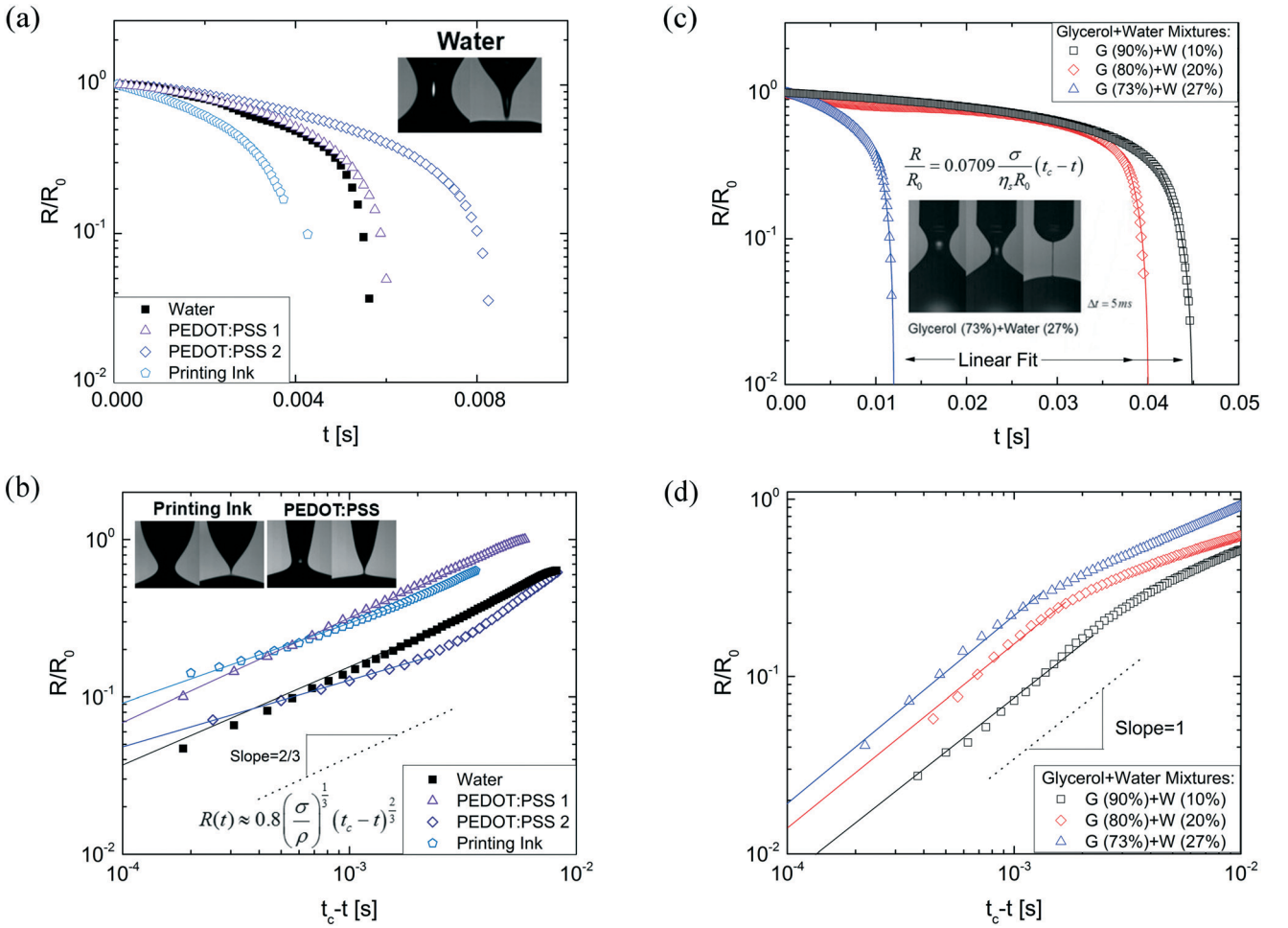

Fig. 2 Neck radius evolution over time for inks, water and water/glycerol mixtures obtained using DoS method: (a) time evolution of scaled radius (ratio of neck radius to nozzle radius) for water and three different inks is shown on a semi-log plot. The liquid neck for water displays the conical shape characteristic of inviscid fluids undergoing capillary-driven thinning and pinch-off. Time step between the two images is 2 ms. (b) Decrease in the scaled radius as the pinch-off instant is approached from the right to the left (time axis is shifted) shown on a log–log plot. Water shows power-law thinning response with an exponent $n = 2/3$ that represents the characteristic slope for inertio-capillary thinning. The two conductive inks (PEDOT:PSS dispersions) thin with exponents of $n = 0.66$ and $n = 0.4$, and the printing ink exhibits $n = 0.5$. Snapshots of the thinning neck are shown for the prinking ink and the PEDOT:PSS 2 dispersion with time step = 2 ms. (c) Radius evolution profiles for high viscosity fluid mixtures of glycerol and water are shown on a semi-log plot. Decreasing volume of glycerol (90%, 80% and 73%) in the mixture leads to lower viscosity and faster pinch-off. (d) Scaled radius profile for the three glycerol–water mixtures shown on log–log plot with the time axis shifted. All three viscous fluids show a linear decay in radius, characteristic of the viscocapillary scaling with t_c = 45 ms, 40 ms and 12 ms respectively.

fluid, shows the characteristic 2/3 scaling anticipated by the potential flow solution or inertio-capillary scaling[81,82] (eqn (1)) shown below:

$$\frac{R(t)}{R_0} \approx 0.8\left(\frac{\sigma}{\rho R_0^3}\right)^{\frac{1}{3}}(t_c - t)^{\frac{2}{3}} = 0.8\left(\frac{t_c - t}{t_R}\right)^{\frac{2}{3}} \quad (1)$$

Here $R(t)$ is the instantaneous radius of the neck, R_0 is outer radius of the nozzle, σ is the surface tension, ρ density of the fluid and t_c is the pinch-off time. The characteristic time for the inertia-dominated neck thinning is given by Rayleigh time $t_R = (\rho R_0^3/\sigma)^{1/2}$, which is also the oscillation time scale for inviscid drops.[1,39,83] Rayleigh time provides an estimate for pinch-off time or processability timescale, and it exhibits a strong dependency on nozzle radius. For experiments described here, $t_R \sim 1$ ms (assuming surface tension of water). The values of pinch-off time, t_c are 4.3 ms for the printing ink, 6 ms for PEDOT:PSS 1, 8.3 ms for PEDOT:PSS 2, and 5.6 ms for water for the dataset shown in Fig. 2.

To illustrate the influence of increase in shear viscosity on capillary thinning dynamics, we analyze the neck radius evolution data sets for three glycerol–water mixtures as shown in Fig. 2(c). Increasing viscosity by increasing the volume fraction of glycerol changes the neck shape: the neck thins to a cylindrical fluid element, in contrast to the conical shape realized for low viscosity systems (Fig. 2a). Furthermore, the radius evolution datasets for these higher viscosity glycerol–water mixtures appear to show a linear decrease in neck radius with time, and the thinning dynamics follow Papageorgiou's viscocapillary scaling[84,85] described by the following expression:

$$\frac{R}{R_0} = 0.0709\frac{\sigma}{\eta_s R_0}(t_p - t) = \left(\frac{t_p - t}{t_v}\right) \quad (2)$$

The characteristic timescale for viscocapillary thinning is given as t_v and it depends on the ratio of capillary stress to viscosity. A dimensionless group called Ohnesorge number,[86] $Oh = t_v/t_R$ defined as the ratio of viscous time to Rayleigh time, provides an estimate of the importance of viscous stress in comparison with inertio-capillary contributions. The inertio-capillary regime is observed for $Oh \ll 1$, and we estimate that for the glycerol–water mixtures shown in Fig. 2c and d, viscous contributions are important as $Oh > 1$. The radius evolution data with 73%, 80% and 90% glycerol respectively yields viscocapillary timescales 5 ms, 8 ms and 12.4 ms, and the pinch-off time, t_c = 11.8 ms, 40 ms and 44.8 ms. The viscocapillary time increases with an increase in shear viscosity, correlating well with the increase in the glycerol fraction (in Fig. 2c and d). The measured values of capillary velocity (ratio of surface tension and viscosity) are comparable to the values obtained using CaBER device by McKinley and Tripathi,[85] and to the capillary velocity computed using the nominal surface tension and viscosity values.

Unlike water and glycerol–water mixtures, the radius evolution for the inks appears to display a power law near pinch-off, fit by $R(t) = Y(t_c - t)^n$ with exponent values, $n < 2/3$. The particle-laden graphic ink shows a power law index of $n = 0.5$. In contrast, the radius evolution data of two conductive inks, PEDOT:PSS 1 (0.22–0.3 wt%) and PEDOT:PSS 2 (0.57–0.75 wt%) respectively display power law index of n = 0.66 and 0.4 respectively. Clearly, the observed difference between the neck shape and pinch-off dynamics between inks and water cannot be attributed to the influence of higher viscosity. The graphic inks are typically low viscosity, multicomponent suspensions that contains pigments (and dyes as colorants), surfactants (as dispersants), polymers and resins (as rheology modifiers, binders and film-formers) that can affect their rheological response. Only a few studies have investigated the influence of added particles.[77,87–89] In spite of a large effort dedicated to synthesis and characterization of printable photovoltaics,[4,7,8,19–23] perhaps due to a lack of suitable techniques, there are few, if any, studies on characterization of capillary-driven self-thinning and pinch-off dynamics, and printability of photovoltaic inks. Hoath and coworkers[90] recently showed that their PEDOT:PSS solutions (made from a different starting stock solution) exhibit shear thinning, and attributed the suppression of satellite drop formation to delayed pinch-off. The shape and scaling law for the inkjet printer ink and two PEDOT:PSS conductive inks determined from DoS rheometry seem to correspond to the power-law scaling exhibited by shear thinning, power law fluids (detailed in a later section). The DoS rheometry characterization of pinch-off dynamics of PEDOT:PSS suspensions highlight researchers can emulate our set-up and analysis to tune and investigate the printability and processability of their unconventional, functional inks.

Elastocapillary thinning and extensional rheology of polymer solutions

The low viscosity systems, including inks described in previous section and dilute aqueous solutions of poly(ethylene oxide) characterized in our previous contribution,[46] require the use of high speed imaging cameras. Here we show that a commercial digital camera (Digital Single Lens Reflex (DSLR) camera, frame rate ≤60 fps or time steps ≥0.0167 s) can be utilized for measuring the concentration-dependent extensional rheology response of viscous, semi-dilute polymer solutions of poly(acrylamide) (PAM) solutions prepared in a high viscosity solvent mixture of glycerol/water (70/30%). The pure solvent exhibits viscocapillary thinning.

The radius evolution in time (Fig. 3) for semi-dilute polyacrylamide solutions in higher viscosity solvent mixture exhibit two regimes: an initial viscocapillary regime (VC) or power law (PL) regime, followed by the elastocapillary thinning that sets in when polymer stretching, orientation and conformational changes contribute additional tensile elastic stresses, $\eta_E\dot{\epsilon}$ in the neck that oppose the capillary stress, σ/R. A slower frame rate in DSLR camera results in fewer data

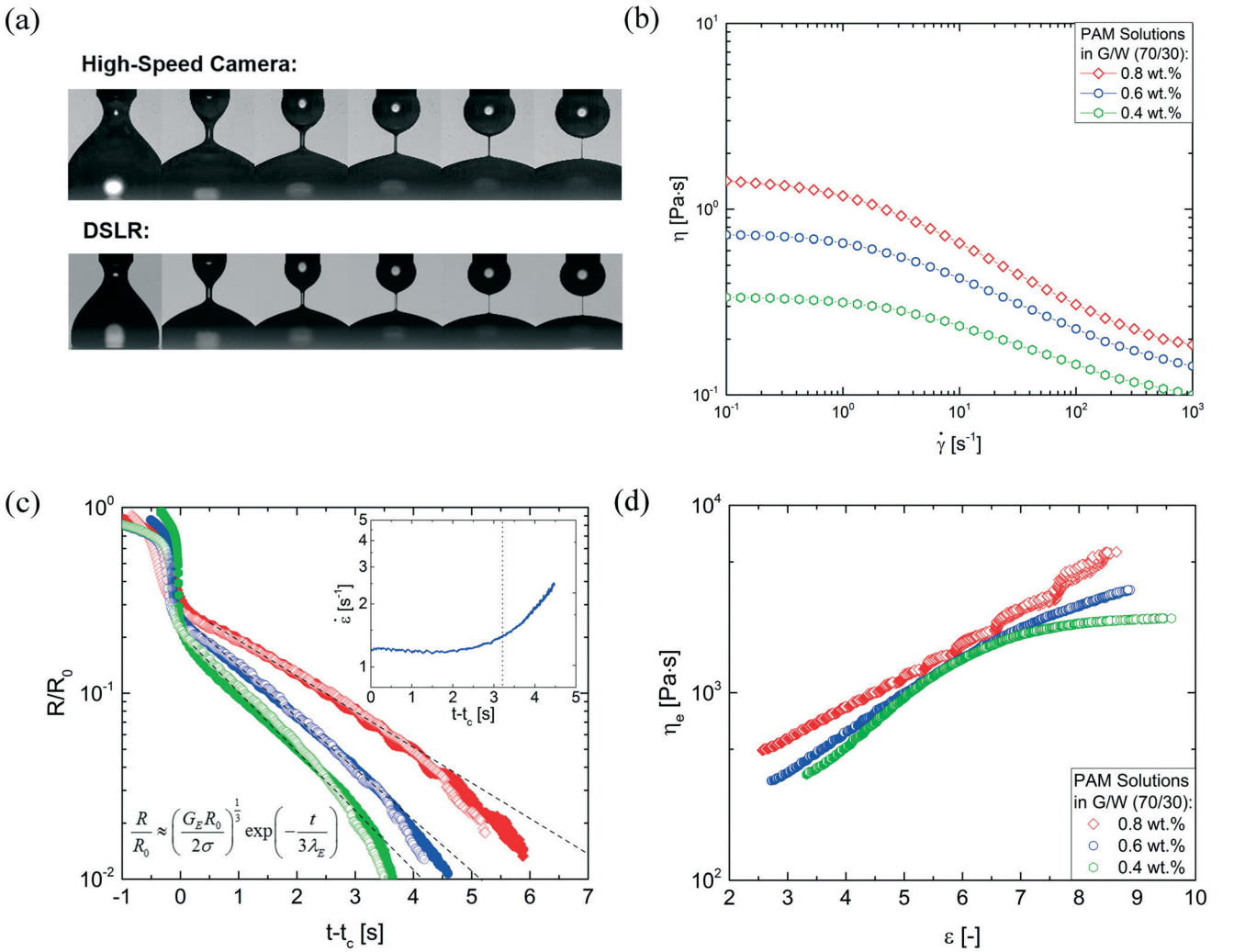

Fig. 3 Characterizing elastocapillary thinning dynamics using DoS technique for semi-dilute polyacrylamide solutions. Data is shown for three different concentrations of PAM (M_w = 5–6 MDa; c^* = 0.067 wt%) in glycerol/water mixture (70/30). (a) Sequences of images show thinning dynamics of PAM 1 wt% solution obtained with high-speed camera (250 fps) and DSLR camera. Time step between images is 2 s. (b) Shear viscosity measurement show a pronounced shear-thinning behavior for deformation rates exceeding 1 s^{-1}. (c) Radius evolution in time: high speed imaging data (closed symbols) and DSLR data (open symbols) are well matched. Pinch-off time increases with concentration. The dashed line shows the fitted region that can be described by the equation shown and corresponds to constant apparent extension rate. The inset shows the typical extension rate variation over time, as evaluated for 0.6% PAM. (d) Extensional viscosity as a function of Hencky strain is found to be 10^2–10^4 times the zero shear viscosity.

points, but the elastocapillary regime is captured quite well as shown in Fig. 3. The filament thinning dynamics in the elastocapillary regime is described using an approximate equation:[44,91]

$$\frac{R(t)}{R_0} \approx \left(\frac{G_E R_0}{2\sigma}\right)^{1/3} \exp\left[-t/3\lambda_E\right] \quad (3)$$

where G_E and λ_E are the elastic modulus and the extensional relaxation time, respectively. In the elastocapillary regime, a homogeneous extensional flow is established within the neck, with an extension rate, $\dot{\varepsilon} = -2\mathrm{d}\ln R(t)/\mathrm{d}t$ that can be computed from the radius evolution plots. The transient extensional viscosity can be evaluated using the following formula:

$$\eta_E = \frac{\sigma}{\dot{\varepsilon} R} = \frac{\sigma}{-2\,\mathrm{d}R(t)/\mathrm{d}t} \quad (4)$$

A constant but fairly large extension rate ($\dot{\varepsilon} = O(10^2$–$10^4)$ s^{-1})) set entirely by the intrinsic polymer dynamics is manifested in the elastocapillary regime. The Hencky strain, $\varepsilon = 2\ln(R_0/R(t))$, increases with time. Increase in polymer fraction leads to an increase in both extensional viscosity and the total strain reached before pinch-off, as shown in Fig. 3d. As the shear viscosity of these semi-dilute aqueous solutions is $0.1 < \eta \leq 2$ Pa s, relatively high Trouton ratios, Tr = 10^2–10^4 are manifested in these experiments. The extensional relaxation time extracted from the elastocapillary fits for the three PAM solutions are respectively 0.5 s, 0.56 s and 0.76 s. The measured

values of extensional relaxation times are quite similar to the timescale estimated from the onset of shear thinning in shear rate-dependent viscosity data for these semi-dilute PAM solutions. Previous studies on semi-dilute unentangled and entangled polymer solutions carried out using CaBER show that the ratio of extensional to shear relaxation times λ_E/λ_S is less than one[92,93] and the ratio decreases with an increase in polymer concentration. In contrast, dilute solutions display extensional relaxation times that are 1–100 times the relaxation time estimated by molecular theory or inferred from shear rheometry.[44–46,49,73,74,92–95] Stretching and orientation of polymer chains in response to an extensional flow field affects both intermolecular interactions and conformation-dependent drag,[95] and contribute to the concentration-dependent increase in the ratio λ_E/λ_S in the dilute solutions and decrease in semi-dilute solutions.

The extensional relaxation time and extensional viscosity of the PAM solutions is two-three orders of magnitude higher than the values obtained for aqueous PEO solutions in our previous contribution.[46] For the dilute aqueous PEO solutions (with relatively low shear viscosity $\eta \leq 2$ mPa s), we recently showed[46] that sub-millisecond relaxation times (or shorter, if higher frame rates $>10^4$ fps are accessible) can be measured using DoS rheometry. Measurement of such short relaxation times are inaccessible in most commercially-available shear and extensional rheometers and there are only a few measurements of such low relaxation times in the open literature.[45,46,72,80] Apart from the advantage of measuring extremely short timescales using high speed imaging for weakly viscoelastic fluids, DoS rheometry protocols present the possibility of an inexpensive measurement of the characteristic timescale for more viscous polymer solutions with off-the-shelf digital cameras and even cellphone cameras.

Dispensing food materials: pinch-off dynamics of power law fluids

Many food materials are emulsions, particle dispersions or foams, *i.e.* complex fluids with a highly non-Newtonian rate-dependent shear viscosity behavior often fit by a power law, and an apparent yield stress.[96] For a power law fluid, the variation of shear stress $\tau = K\dot{\gamma}^n$ with shear rate is described using the power law index, n and the flow consistency, K. While the effect of polymers on pinch-off dynamics and their conformational changes in response to extensional flow are relatively well-understood,[44,97] many unanswered questions remain in understanding of, and control over, pinch-off dynamics of multicomponent complex fluids with complex microstructure and power-law rheology. Using DoS rheometry, we characterize the pinch-off dynamics of four fluids that exhibit shear thinning response at high shear rates, including two food materials (ketchup and mayonnaise), and two model power law fluids: Carbopol solutions (0.15% and 0.25% by weight, provided by the Ewoldt group). Ketchup is a suspension of tomato pulp and spices (with salt, sugar and preservatives added) in a continuous phase that is designed with thickening agents, usually polysaccharide hydrocolloids, dissolved in water to improve the consistency, stability and rheology of ketchup.[98–100] Mayonnaise is an emulsion, and carbopol in water has a microstructure that comprises of swollen, elastic microsponge-like particles (2–20 μm). Most rheological studies performed on ketchup and other food materials focus on their complex response to shear flows,[98–100] and on how to quantify and control yield stress, thixotropy, shear thinning at high shear rates to control their flow behavior and processability. Here we examine their flow behavior using DoS rheometry, which emulates the deformation flow fields encountered in daily dispensing, drop formation as well as industrial bottle filling processes. Radius evolution data in time, measured using DoS rheometry, are shown in Fig. 4.

The radius evolution equation for power law fluids can be represented as:

$$\frac{R}{R_0} = Y(t_c - t)^n = \left(\frac{t_c - t}{t_{PL}}\right)^n \quad (5)$$

Doshi *et al.*[101] showed that it is possible to define $Y = \Phi(n)\sigma/K = t_{PL}^{-n}$ for $n > 0.6$. The timescale t_{PL} represents the characteristic timescale for power law fluids. The pinch-off dynamics of power law fluids with $n < 0.6$ also exhibit a power law behavior, as shown by numerically computed profiles obtained by Suryo and Basaran[102] (termed as non-slender viscous power law (NSVP) scaling) and in CaBER experiments from Huisman *et al.*[103] Fitting the radius evolution profiles using eqn (5) gives the values of $n = 0.28$ for ketchup, $n = 0.36$ for mayonnaise and $n =$ (0.18 and 0.2) for the two Carbopol solutions. All the chosen fluids show power law rheology and shear thinning behavior ($n < 1$), see Table 1. For power law fluids with $n < 0.6$, though an analytical relationship between the pre-factor Y, and model parameters n and K is not known, Table 1 lists the values of prefactor Y, power law index n and pinch-off time, t_c obtained from the fits to the radius evolution data. The power law exponents obtained using DoS Rheometry exhibit reasonable agreement with our shear thinning data for ketchup, the value $n = 0.24$ obtained by Coussot and Gaulard[104] using Herschel–Buckley model fits to ketchup shear rheology data, the power law exponents for Carbopol solutions obtained by the Ewoldt group using steady shear viscosity data, (all included in Table 1) and the power law exponent obtained for mayonnaise by Huisman *et al.*[103] using CaBER.

Even though aspect ratio and nozzle size (plate diameter) do not affect the response measured for polymer solutions in DoS Rheometry (CaBER) measurements, a detailed investigation of the influence of such parameters is warranted for power law fluids. Though our preliminary experiments with power law fluids show a reasonable repeatability, a substantial increase in the distance between nozzle and substrate is

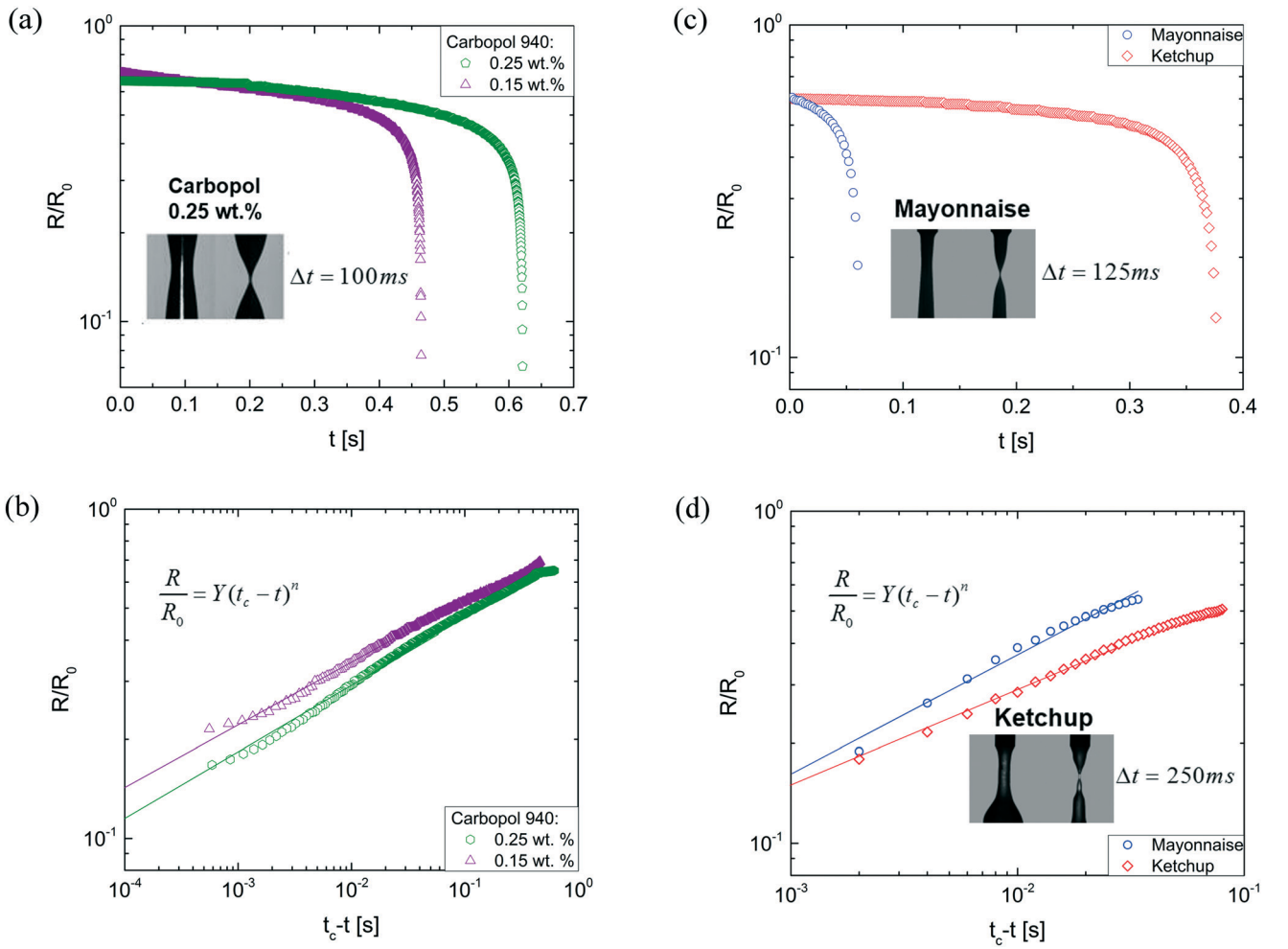

Fig. 4 Rheological measurements of Carbopol solutions and food materials, examples of power law fluids: (a) radius evolution of two Carbopol solutions, shown on semi-log scale to highlight the contrast with the elastocapillary thinning behavior. The snapshots show that neck thins down to form two axisymmetric cones characteristic of the non-slender viscous power law behavior. (b) Radius evolution plot for the two Carbopol solutions show power law behavior, plotted here on a log–log scale. (c) Radius evolution plot for ketchup and mayonnaise, plotted here on a semi-log scale. Though the initial thinning rate is relatively slow for such high viscosity fluids, the thinning rate diverges before pinch-off. (d) Radius evolution plot for ketchup and mayonnaise show power law behavior, plotted here on a log–log scale, with shifted time. The exponent obtained for ketchup using filament thinning data (n = 0.28) is in good agreement with the power law index obtained from shear viscosity measurements.

necessary to create an unstable liquid bridge, which is consistent with the previous observations.[104–108] In the viscous power law fluids, it is evident that the formation of a neck (attached to a pendant droplet) requires an initial gravity-driven drainage regime; indeed the initial configuration and thinning behavior can be considered to be similar to the dripping experiments. After a neck forms, pumping is stopped even before the suspended drop contacts the underlying substrate. The last stage of filament thinning occurs in a stretched liquid bridge bounded by a drop each at the nozzle and on the substrate. Thus in the late stage of filament thinning, fit here by a power law, the liquid bridge configuration and dynamics are similar to those realized in CaBER measurements, and in the late stage, capillary stresses drive the outward flow from the thinning neck.

Coussot and Gaulard[104] investigated at the length of separation of ketchup, mayonnaise and mineral suspension from a nozzle as drops fell under their own weight, and found that the separation length and drop size are nearly independent of flow rates below a critical pumping rate. Likewise, using experiments involving liquid bridges stretched between two

Table 1 Comparison of power law indices obtained by fitting rate-dependent response of steady shear viscosity using a torsional rheometer and radius evolution profile using DoS rheometry

	Shear rheology		DoS rheometry		
Fluid	K	n	Y	n	t_c [s]
Carbopol 0.15 wt%	43.7	0.18	0.78	0.18	0.46
Carbopol 0.25 wt%	109.6	0.15	0.75	0.20	0.62
Ketchup	11.8	0.26	1.07	0.28	0.38
Conditioner	17.6	0.12	0.82	0.17	0.1
Mayonnaise	60.5	0.36	1.93	0.36	0.06
Bentonite 2.4 wt%	—	—	1.06	0.19	0.49

glass plates with varying velocity, Louvet *et al.*[107] showed that for slow stretch experiments, the filament thinning dynamics can be understood using constitutive relations developed for describing shear rheology response and by using scaling laws developed for yield stress fluids; however, a nonuniversal behavior is observed at faster stretching rates. Our preliminary experiments show a similar pumping rate-independent dynamics for the low flow rate(s) used. Like Huisman *et al.*[103] we find that many power law fluids do exhibit same power law exponent in their shear thinning response measured using torsional shear rheometer and in filament thinning during pinch-off measured with DoS rheometry. Nevertheless, the complex interplay of yield stress, shear thinning, thixotropy, deformation history, competition between surface tension and yield stress, as well as role of gravity in creating an unstable neck, leading to pinch-off are all challenging problems that require further investigation.

Pinch-off dynamics of multicomponent complex fluids in cosmetic industry

Next we compare the shear rheology and pinch-off dynamics of three hair products with similar brand name and ingredients: a shampoo, a conditioner and a blend of both called 2 in 1 manufactured by the same parent company (Pantene, manufactured by P&G). All the three fluids contain a large amount of added surfactants (high enough concentration to form wormlike micelles) in addition to ingredients that primarily influence color, fragrance *etc.* Both conditioner and 2 in 1 additionally contain polysaccharide-based thickeners added for modifying the rheological response and processability/dispensability. The three hair products exhibit similar shear thinning response in steady shear measurements made using cone and plate geometry on Anton Paar MCR 302 torsional rheometer. The three fluids show a power

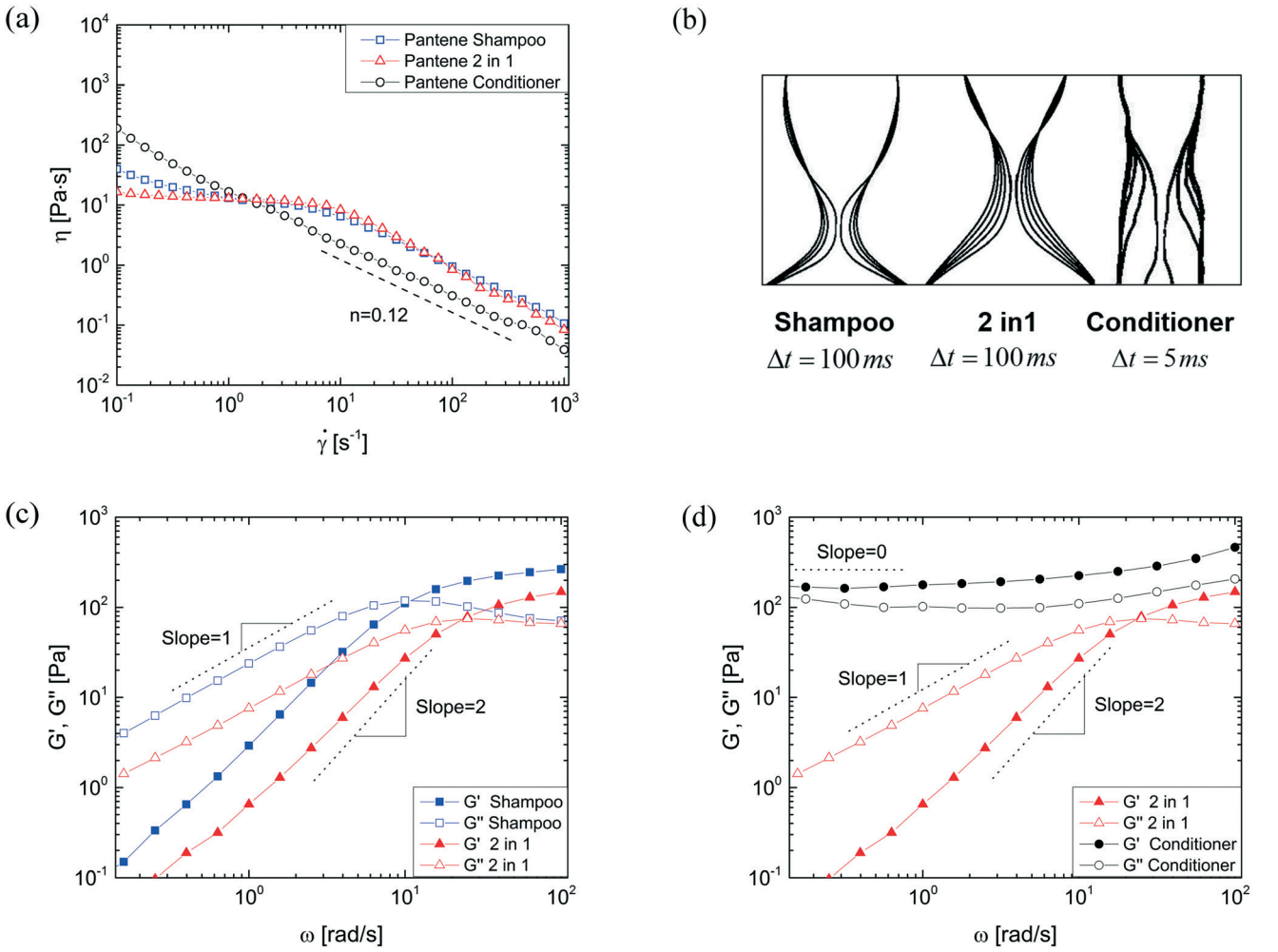

Fig. 5 Shear and extensional rheology of commercial brand cosmetic products (shampoo, conditioner and 2 in 1): (a) shear viscosity measurements for three different fluids showing very similar behavior for shampoo and 2 in 1 in shear flow. (b) Filament profile close to the pinch-off for three different classes of fluid: shampoo (viscous), 2 in 1 (viscoelastic) and conditioner (power law) fluids. (c) The storage modulus $G' \sim \omega^2$ and the loss modulus $G'' \sim \omega$ show characteristic frequency dependence for viscoelastic fluids for shampoo and 2 in 1. (d) Conditioner shows gel-like response, with modulus values that are frequency independent.

law index, n = 0.12 (see Fig. 5), though the conditioner has the highest zero shear viscosity among the three fluids. Furthermore, as the rate-dependent viscosity response of the three fluids is quite similar, most processing models used for designing pumping rate or fill rate for bottles that rely on shear rheology data will return similar processing parameters for these three fluids. However, pouring, pumping through converging channels, dispensing, formation of droplets or transfer of cosmetics from bottle to palm involve extensional flow fields, and therefore in addition to shear rheology response, we must characterize their extensional response for assessing their processability and dispensing behavior. The dripping-onto-substrate experiments show strikingly distinct neck shape profiles (see Fig. 5b). In all the power law fluids described earlier, pinch-off occurs from a non-slender liquid bridge configuration resulting in the formation of two axisymmetric cones after break-up. The filament thinning in shampoo, 2 in 1 and conditioner is qualitatively different from the other power law fluids.

We examined the linear viscoelastic response of the three fluids using small amplitude oscillatory shear measurements. While shampoo and 2 in 1 behaved like viscoelastic fluids, with the storage modulus $G' \sim \omega^2$ and the loss modulus $G'' \sim \omega$ showing characteristic frequency dependence respectively, the conditioner showed a typical viscoelastic solid behavior as both storage and loss modulus are nearly frequency-independent. The crossover frequency, ω_c can be estimated from it have similar values for shampoo and 2 in 1. Nevertheless, the dripping-onto-substrate experiments show three strikingly distinct radius evolution profiles (see Fig. 6). The shampoo displays a viscocapillary thinning (see eqn (2)) and the 2 in 1 sample shows an elastocapillary regime (eqn (3)) before pinch-off. The power law exponent, n = 0.17 exhibited by radius evolution data for conditioner. However, the neck shape (Fig. 5b) before pinch-off dynamics of conditioner as well as of ketchup appears to produce axisymmetric cones characteristic of NSVP scaling only in some cases.

The neck shapes observed for shampoo and 2 in 1 repeatedly show formation of a cylindrical filament that drains quite slowly and in the case of 2 in 1, even beads-on-a-string structure forms in the last stage. The shape of the neck before pinch-off for 2 in 1, ketchup and conditioner are included in a pictogram displayed as Fig. 7 that showcases the primary neck shapes obtained for a wide spectrum of complex fluids. A careful examination of Fig. 7 reveals that even the images (a few movies are included as ESI† online) contain distinct features that can be helpful in judging if the fluid response can be described as inertio-capillary, viscocapillary, power law or elastocapillary.

Chocolate syrup, molasses, glycerol, honey and egg yolk all show viscocapillary thinning. Clay suspensions (bentonite suspensions), hand cream, mayonnaise, and carbopol solutions are all materials designed to flow on application of stress or high flow rate and then to deposit on a substrate with minimal spreading (revert to high viscosity at low rates), are ideal for many dispensing applications. The pinch-off dynamics for such materials exhibits formation of two distinct cones, while inviscid fluids like water exhibit a single cone (see Fig. 7). The micrographs for two PEO solutions (M_w = 1 × 10^6 Da, c^* = 0.17% by weight) shown in Fig. 7 show the cylindrical filament associated with elastocapillary thinning. DoS rheometry results with aqueous PEO solutions were detailed in an earlier contribution.[46] In addition to the examples presented in this study, there is potential to use DoS rheometry for quantifying pinch-of dynamics, extensional rheology and printability of shear thickening fluids,[60,109] polymer solutions used for fiber spinning,[110–112] smectic

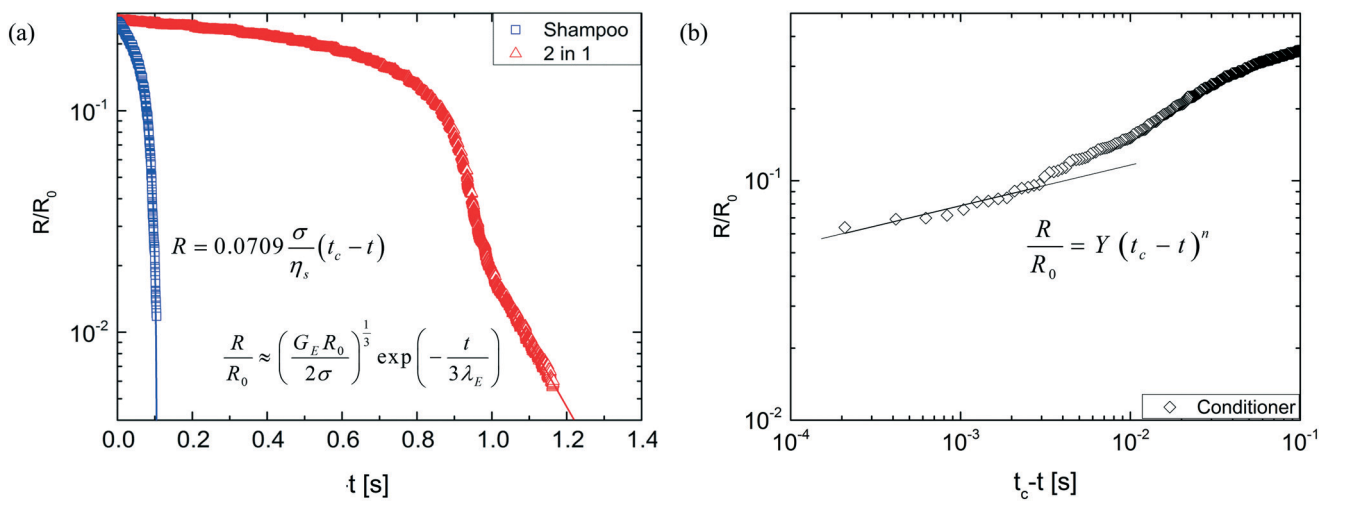

Fig. 6 DoS rheometry of cosmetic products (shampoo, conditioner and 2 in 1): (a) radius evolution of the fluid filament in extensional flow field form shampoo and 2 in 1. Despite exhibiting similar behavior in response to shear flow, the two fluids show a noticeably different behavior in their response to extensional flow. (b) Radius evolution of conditioner over time shows power-law scaling, with n = 0.17.

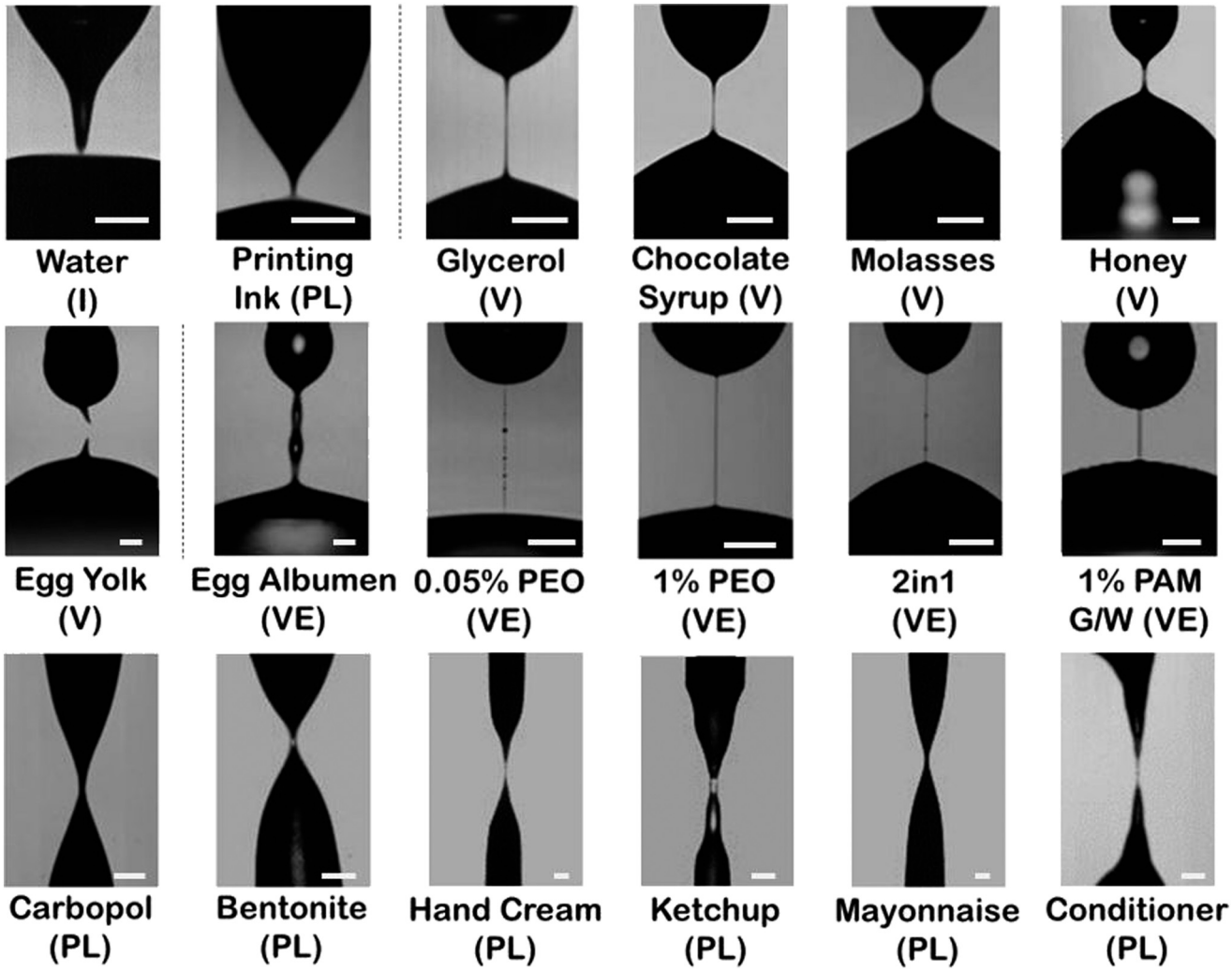

Fig. 7 Assessing pinch-off dynamics and printability of complex fluids using dripping-onto-substrate rheometry: images show DoS rheometry characterization of different classes of fluids including inviscid (I), viscous (V), viscoelastic (VE) and power law (PL) fluids. Each snapshot captured with high-speed camera shows the characteristic neck profile observed for these fluids moments before the final pinch-off. Scale bar corresponds to 0.5 mm.

liquid crystals,[113] surfactant-laden fluids[114] and foams;[103] the reference studies that were carried out with CaBER and dripping, show rich and complex behavior.

IV. Conclusions

Visualization and analysis of the capillary-driven thinning and pinch-off dynamics provides a quantitative measure of extensional viscosity and characteristic processability time, and industrially-relevant assessment of drop formation for microfluidics and printing applications. In this paper, using dripping-onto-substrate set-up, we examined the capillary-thinning and pinch-off dynamics of several model fluids that exhibit characteristic response expected for inviscid, viscous, power law and viscoelastic fluids respectively. The DoS rheometry implemented with a commercial digital camera (or cellphone) can be used for measuring viscosity of Newtonian fluids like honey, molasses and chocolate syrup. Likewise, we find that many cosmetics and food materials show power law response to both shear flow and extensional flow. Unlike CaBER, DoS rheometry is suitable for accessing the pinch-off dynamics of low viscosity ($\eta < 20$ mPa s), low elasticity ($\lambda < 1$ ms) fluids, and quantifying concentration-dependent extensional rheology for aqueous polymer solutions. In our previous contribution that introduces DoS rheometry,[46] we characterized pinch-off dynamics of aqueous polymer solutions, and measured extensional relaxation time and extensional viscosity for low viscosity ($\eta < 20$ mPa s), low elasticity ($\lambda < 1$ ms) systems to highlight the suitability of the protocols for extremely low viscosity, low elasticity fluids. Here we show the DoS rheometry technique can be also applied for studying the pinch-off dynamics of low viscosity inks.

Our experiments suggest that even simple visualization of shapes provides a possibility for a quick assessment of the likely rheological response of multicomponent mixtures. We find that the visualization of a single drop onto a substrate (repeated more than five times per sample for checking repeatability) is sufficient to provide both qualitative and

quantitative assessment of the flow behavior and printability of complex fluids. We show that it is possible to quantify shear (and extensional) viscosity of Newtonian fluids with the dripping-onto-substrate technique, and is it possible to do so in an economical, quick and reliable manner. We examine the characteristics of pinch-off dynamics in food and cosmetic materials, and show that it is possible to design fluids with similar shear viscosity response, but dramatically different pinch-off dynamics. We contend that since the DoS rheometry protocols, can be replicated and emulated relatively easily and quite inexpensively for high viscosity fluids, the present contribution will enable both design of printable materials, and inspire much needed studies on microstructure-dependent material properties that influence pinch-off dynamics and extensional rheology of complex fluids. The present contribution will allow formulators, printers, researchers and processing engineers with tests and understanding of how the processability (often described in heuristic terms such as printability, sprayability, spinnability and jettability) of complex fluids is influenced and determined by their rheological response. This is crucial for designing materials for printing applications or identifying the most suitable processing conditions for optimized material combinations.

Acknowledgements

We will like to acknowledge Jeremy Brunette, Kimberly Clark Co. for suggesting a comparison between shampoo, conditioner and 2 in 1 samples. The authors acknowledge contribution by Yiran Zhang to the development of Dripping-onto-Substrate Rheometry protocols. We would like to thank Prof. Randy Ewoldt and his student Arif Nelson, University of Illinois at Urbana-Champaign for providing us with the Carbopol solutions and Bentonite suspension for carrying out the DoS rheometry studies described here. VS thanks the UIC College of Engineering and the Department of Chemical Engineering for start-up funds, and also acknowledges an initiation grant from the Campus Research Board (CRB) at UIC.

References

1 J. Eggers, *Rev. Mod. Phys.*, 1997, **69**, 865–929.
2 O. A. Basaran, *AIChE J.*, 2002, **48**, 1842–1848.
3 O. A. Basaran, H. Gao and P. P. Bhat, *Annu. Rev. Fluid Mech.*, 2013, **45**, 85–113.
4 B. Derby, *Annu. Rev. Mater. Res.*, 2010, **40**, 395–414.
5 S. Kumar, *Annu. Rev. Fluid Mech.*, 2014, **47**, 67–94.
6 J. Sun, B. Bao, M. He, H. Zhou and Y. Song, *ACS Appl. Mater. Interfaces*, 2015, **7**, 28086–28099.
7 F. C. Krebs, *Sol. Energy Mater. Sol. Cells*, 2009, **93**, 394–412.
8 B. Kang, W. H. Lee and K. Cho, *ACS Appl. Mater. Interfaces*, 2013, **5**, 2302–2315.
9 J. Li, F. Rossignol and J. Macdonald, *Lab Chip*, 2015, **15**, 2538–2558.
10 G. F. Christopher and S. L. Anna, *J. Phys. D: Appl. Phys.*, 2007, **40**, R319.
11 C.-H. Choi, J.-H. Jung, D.-W. Kim, Y.-M. Chung and C.-S. Lee, *Lab Chip*, 2008, **8**, 1544–1551.
12 P. Garstecki, M. J. Fuerstman, H. A. Stone and G. M. Whitesides, *Lab Chip*, 2006, **6**, 437–446.
13 R. Seemann, M. Brinkmann, T. Pfohl and S. Herminghaus, *Rep. Prog. Phys.*, 2011, **75**, 016601.
14 S. Köster, F. E. Angile, H. Duan, J. J. Agresti, A. Wintner, C. Schmitz, A. C. Rowat, C. A. Merten, D. Pisignano and A. D. Griffiths, *Lab Chip*, 2008, **8**, 1110–1115.
15 J. F. Edd, D. Di Carlo, K. J. Humphry, S. Köster, D. Irimia, D. A. Weitz and M. Toner, *Lab Chip*, 2008, **8**, 1262–1264.
16 A. R. Abate, J. Thiele and D. A. Weitz, *Lab Chip*, 2011, **11**, 253–258.
17 A. R. Abate and D. A. Weitz, *Lab Chip*, 2011, **11**, 1911–1915.
18 R. K. Shah, H. C. Shum, A. C. Rowat, D. Lee, J. J. Agresti, A. S. Utada, L.-Y. Chu, J.-W. Kim, A. Fernandez-Nieves and C. J. Martinez, *Mater. Today*, 2008, **11**, 18–27.
19 C. N. Hoth, S. A. Choulis, P. Schilinsky and C. J. Brabec, *Adv. Mater.*, 2007, **19**, 3973–3978.
20 C. N. Hoth, P. Schilinsky, S. A. Choulis, S. Balasubramanian and C. J. Brabec, in *Applications of Organic and Printed Electronics*, Springer, 2013, pp. 27–56.
21 J. Alstrup, M. Jørgensen, A. J. Medford and F. C. Krebs, *ACS Appl. Mater. Interfaces*, 2010, **2**, 2819–2827.
22 L. Yang, T. Zhang, H. Zhou, S. C. Price, B. J. Wiley and W. You, *ACS Appl. Mater. Interfaces*, 2011, **3**, 4075–4084.
23 C. A. Wolden, J. Kurtin, J. B. Baxter, I. Repins, S. E. Shaheen, J. T. Torvik, A. A. Rockett, V. M. Fthenakis and E. S. Aydil, *J. Vac. Sci. Technol., A*, 2011, **29**, 030801.
24 V. Subramanian, J. M. J. Frechet, P. C. Chang, D. C. Huang, J. B. Lee, S. E. Molesa, A. R. Murphy and D. R. Redinger, *Proc. IEEE*, 2005, **93**, 1330–1338.
25 H. Sirringhaus, T. Kawase, R. H. Friend, T. Shimoda, M. Inbasekaran, W. Wu and E. P. Woo, *Science*, 2000, **290**, 2123–2126.
26 A. Määttänen, P. Ihalainen, P. Pulkkinen, S. Wang, H. Tenhu and J. Peltonen, *ACS Appl. Mater. Interfaces*, 2012, **4**, 955–964.
27 P. Calvert, *Chem. Mater.*, 2001, **13**, 3299–3305.
28 Y. Luo, D. Zhai, Z. Huan, H. Zhu, L. Xia, J. Chang and C. Wu, *ACS Appl. Mater. Interfaces*, 2015, **7**, 24377–24383.
29 B. Derby, *Science*, 2012, **338**, 921–926.
30 S. V. Murphy and A. Atala, *Nat. Biotechnol.*, 2014, **32**, 773–785.
31 M. M. Stanton, J. Samitier and S. Sánchez, *Lab Chip*, 2015, **15**, 3111–3115.
32 E. M. Hamad, S. E. R. Bilatto, N. Y. Adly, D. S. Correa, B. Wolfrum, M. J. Schöning, A. Offenhäusser and A. Yakushenko, *Lab Chip*, 2016, **16**, 70–74.
33 P. Gao, A. J. Hunter, M. J. Summe and W. A. Phillip, *ACS Appl. Mater. Interfaces*, 2016, **8**(30), 19772–19779.
34 I. Gibson, D. Rosen and B. Stucker, *Additive manufacturing technologies: 3D printing, rapid prototyping, and direct digital manufacturing*, Springer, 2014.
35 E. Tekin, P. J. Smith and U. S. Schubert, *Soft Matter*, 2008, **4**, 703–713.

36 C. A. Wolden, J. Kurtin, J. B. Baxter, I. Repins, S. E. Shaheen, J. T. Torvik, A. A. Rockett, V. M. Fthenakis and E. S. Aydil, *J. Vac. Sci. Technol., A*, 2011, **29**, 030801.
37 J. Eggers and E. Villermaux, *Rep. Prog. Phys.*, 2008, **71**, 036601.
38 *Handbook of Atomization and Sprays: Theory and Applications*, ed. N. Ashgriz, Springer, New York, 2011.
39 S. Middleman, *Modeling Axisymmetric Flows: Dynamics of Films, Jets and Drops*, Academic Press, San Diego, 1995.
40 M. D. Graham, *Phys. Fluids*, 2003, **15**, 1702.
41 H. C. Nallan, J. A. Sadie, R. Kitsomboonloha, S. K. Volkman and V. Subramanian, *Langmuir*, 2014, **30**, 13470–13477.
42 A. L. Yarin, *Free Liquid Jets and Films: Hydrodynamics and Rheology*, Longman Scientific & Technical, 1993.
43 C. Clasen, P. M. Phillips and L. Palangetic, *AIChE J.*, 2012, **58**, 3242–3255.
44 G. H. McKinley, *Rheol. Rev.*, 2005, 1–48.
45 V. Sharma, S. J. Haward, J. Serdy, B. Keshavarz, A. Soderlund, P. Threlfall-Holmes and G. H. McKinley, *Soft Matter*, 2015, **11**, 3251–3270.
46 J. Dinic, Y. Zhang, L. N. Jimenez and V. Sharma, *ACS Macro Lett.*, 2015, **4**, 804–808.
47 S. L. Anna and G. H. McKinley, *J. Rheol.*, 2001, **45**, 115–138.
48 A. Ardekani, V. Sharma and G. H. McKinley, *J. Fluid Mech.*, 2010, **665**, 46–56.
49 V. Tirtaatmadja, G. H. McKinley and J. J. Cooper-White, *Phys. Fluids*, 2006, **18**, 043101.
50 Y. Amarouchene, D. Bonn, J. Meunier and H. Kellay, *Phys. Rev. Lett.*, 2001, **86**, 3558–3561.
51 J. B. Dahl, V. Narsimhan, B. Gouveia, S. Kumar, E. S. Shaqfeh and S. J. Muller, *Soft Matter*, 2016, **12**, 3787–3796.
52 P. Szymczak and M. Cieplak, *J. Phys.: Condens. Matter*, 2010, **23**, 033102.
53 D. E. Smith and S. Chu, *Science*, 1998, **281**, 1335–1340.
54 C. M. Schroeder, H. P. Babcock, E. S. G. Shaqfeh and S. Chu, *Science*, 2003, **301**, 1515–1519.
55 F. T. Trouton, *Proc. R. Soc. London, Ser. A*, 1906, **77**, 426–440.
56 E. Miller, C. Clasen and J. P. Rothstein, *Rheol. Acta*, 2009, **48**, 625–639.
57 J. P. Rothstein, *Rheol. Rev.*, 2008, 1–46.
58 J. P. Rothstein, *J. Rheol.*, 2003, **47**, 1227–1247.
59 N. J. Kim, C. J. Pipe, K. H. Ahn, S. J. Lee and G. H. McKinley, *Korea-Aust. Rheol. J.*, 2010, **22**, 31–41.
60 M. Chellamuthu, E. M. Arndt and J. P. Rothstein, *Soft Matter*, 2009, **5**, 2117–2124.
61 A. W. K. Ma, F. Chinesta, T. Tuladhar and M. R. Mackley, *Rheol. Acta*, 2008, **47**, 447–457.
62 D. E. Tsentalovich, A. W. K. Ma, J. A. Lee, N. Behabtu, E. A. Bengio, A. Choi, J. Hao, Y. Luo, R. J. Headrick, M. J. Green, Y. Talmon and M. Pasquali, *Macromolecules*, 2016, **49**, 681–689.
63 A. Bazilevsky, V. Entov and A. Rozhkov, presented in part at the *Third European Rheology Conference and Golden Jubilee Meeting of the British Society of Rheology*, Edinburgh, UK, 1990.
64 A. V. Bazilevskii, V. M. Entov and A. N. Rozhkov, *Polym. Sci., Ser. A*, 2001, **43**, 716–726.
65 A. V. Bazilevsky, V. M. Entov and A. N. Rozhkov, *Fluid Dyn.*, 2011, **46**, 613–622.
66 M. Stelter, G. Brenn, A. L. Yarin, R. P. Singh and F. Durst, *J. Rheol.*, 2000, **44**, 595–616.
67 M. Stelter, G. Brenn, A. L. Yarin, R. P. Singh and F. Durst, *J. Rheol.*, 2002, **46**, 507–527.
68 L. E. Rodd, T. P. Scott, J. J. Cooper-White and G. H. McKinley, *Appl. Rheol.*, 2005, **15**, 12–27.
69 G. H. McKinley, *Rheol. Rev.*, 2005, 1–48.
70 P. Schummer and K. H. Tebel, *Rheol. Acta*, 1982, **21**, 514–516.
71 P. Schummer and K. H. Tebel, *J. Non-Newtonian Fluid Mech.*, 1983, **12**, 331–347.
72 B. Keshavarz, V. Sharma, E. C. Houze, M. R. Koerner, J. R. Moore, P. M. Cotts, P. Threlfall-Holmes and G. H. McKinley, *J. Non-Newtonian Fluid Mech.*, 2015, **222**, 171–189.
73 Y. Christanti and L. M. Walker, *J. Non-Newtonian Fluid Mech.*, 2001, **100**, 9–26.
74 Y. Christanti and L. M. Walker, *J. Rheol.*, 2002, **46**, 733–748.
75 J. J. Cooper-White, J. E. Fagan, V. Tirtaatmadja, D. R. Lester and D. V. Boger, *J. Non-Newtonian Fluid Mech.*, 2002, **106**, 29–59.
76 C. Wagner, Y. Amarouchene, D. Bonn and J. Eggers, *Phys. Rev. Lett.*, 2005, 95.
77 R. J. Furbank and J. F. Morris, *Int. J. Multiphase Flow*, 2007, **33**, 448–468.
78 C. A. Schneider, W. S. Rasband and K. W. Eliceiri, *Nat. Methods*, 2012, **9**, 671–675.
79 J. Plog, W. Kulicke and C. Clasen, *Appl. Rheol.*, 2005, **15**, 28–37.
80 L. Campo-Deano and C. Clasen, *J. Non-Newtonian Fluid Mech.*, 2010, **165**, 1688–1699.
81 R. F. Day, E. J. Hinch and J. R. Lister, *Phys. Rev. Lett.*, 1998, **80**, 704–707.
82 J. R. Castrejón-Pita, A. A. Castrejón-Pita, S. S. Thete, K. Sambath, I. M. Hutchings, J. Hinch, J. R. Lister and O. A. Basaran, *Proc. Natl. Acad. Sci. U. S. A.*, 2015, **112**, 4582–4587.
83 L. Rayleigh, *Proc. R. Soc. London*, 1879, **29**, 71–97.
84 D. T. Papageorgiou, *Phys. Fluids*, 1995, **7**, 1529–1544.
85 G. H. McKinley and A. Tripathi, *J. Rheol.*, 2000, **44**, 653–670.
86 G. H. McKinley and M. Renardy, *Phys. Fluids*, 2011, **23**, 127101.
87 P. J. Zimoch, G. H. McKinley and A. E. Hosoi, *Phys. Rev. Lett.*, 2013, **111**, 036001.
88 T. Bertrand, C. Bonnoit, E. Clément and A. Lindner, *Granular Matter*, 2012, 1–6.
89 C. Bonnoit, T. Bertrand, E. Clément and A. Lindner, *Phys. Fluids*, 2012, **24**, 043304.
90 S. D. Hoath, S. Jung, W.-K. Hsiao and I. M. Hutchings, *Org. Electron.*, 2012, **13**, 3259–3262.
91 V. M. Entov and E. J. Hinch, *J. Non-Newtonian Fluid Mech.*, 1997, **72**, 31–54.
92 O. Arnolds, H. Buggisch, D. Sachsenheimer and N. Willenbacher, *Rheol. Acta*, 2010, **49**, 1207–1217.
93 D. Sachsenheimer, B. Hochstein and N. Willenbacher, *Rheol. Acta*, 2014, **53**, 725–739.

94 C. Clasen, J. P. Plog, W. M. Kulicke, M. Owens, C. Macosko, L. E. Scriven, M. Verani and G. H. McKinley, *J. Rheol.*, 2006, **50**, 849–881.
95 R. Prabhakar, S. Gadkari, T. Gopesh and M. J. Shaw, *J. Rheol.*, 2016, **60**, 345–366.
96 R. G. Larson, *The Structure and Rheology of Complex Fluids*, Oxford University Press, New York, 1999.
97 R. G. Larson, *J. Rheol.*, 2005, **49**, 1–70.
98 L. Juszczak, Z. Oczadły and D. Gałkowska, *Food Bioprocess Technol.*, 2013, **6**, 1251–1260.
99 A. Koocheki, A. Ghandi, S. Razavi, S. A. Mortazavi and T. Vasiljevic, *Int. J. Food Sci. Technol.*, 2009, **44**, 596–602.
100 H. S. Gujral, A. Sharma and N. Singh, *Int. J. Food Prop.*, 2002, **5**, 179–191.
101 P. Doshi, R. Suryo, O. E. Yildirim, G. H. McKinley and O. A. Basaran, *J. Non-Newtonian Fluid Mech.*, 2003, **113**, 1–27.
102 R. Suryo and O. A. Basaran, *J. Non-Newtonian Fluid Mech.*, 2006, **138**, 134–160.
103 F. M. Huisman, S. R. Friedman and P. Taborek, *Soft Matter*, 2012, **8**, 6767–6774.
104 P. Coussot and F. Gaulard, *Phys. Rev. E: Stat., Nonlinear, Soft Matter Phys.*, 2005, **72**, 031409.
105 G. German and V. Bertola, *Phys. Fluids*, 2010, **22**, 033101.
106 L. Martinie, H. Buggisch and N. Willenbacher, *J. Rheol.*, 2013, **57**, 627–646.
107 N. Louvet, D. Bonn and H. Kellay, *Phys. Rev. Lett.*, 2014, **113**, 218302.
108 K. Niedzwiedz, O. Arnolds, N. Willenbacher and R. Brummer, *Appl. Rheol.*, 2009, **19**, 41969.
109 E. E. B. White, M. Chellamuthu and J. P. Rothstein, *Rheol. Acta*, 2009, **49**, 119–129.
110 L. Palangetic, N. K. Reddy, S. Srinivasan, R. E. Cohen, G. H. McKinley and C. Clasen, *Polymer*, 2014, **55**, 4920–4931.
111 Y. Fang, A. D. Dulaney, J. Gadley, J. M. Maia and C. J. Ellison, *Polymer*, 2015, **73**, 42–51.
112 S. J. Haward, V. Sharma, C. P. Butts, G. H. McKinley and S. S. Rahatekar, *Biomacromolecules*, 2012, **13**, 1688–1699.
113 J. R. Savage, M. Caggioni, P. T. Spicer and I. Cohen, *Soft Matter*, 2010, **6**, 892–895.
114 M. Roché, M. Aytouna, D. Bonn and H. Kellay, *Phys. Rev. Lett.*, 2009, **103**, 264501.